

# Electron Transport in Dye-Sensitized TiO<sub>2</sub> Nanowire Arrays in Contact with Aqueous Electrolytes

Langqiu Xiao, Yanan Yu, Emma L. Schultz, Eric A. Stach, and Thomas E. Mallouk\*

Cite This: *J. Phys. Chem. C* 2020, 124, 22003–22010

Read Online

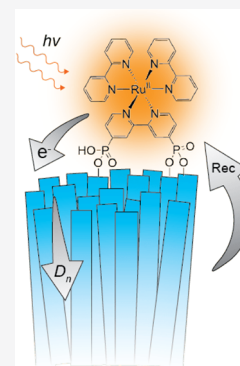
ACCESS |

Metrics &amp; More

Article Recommendations

Supporting Information

**ABSTRACT:** In aqueous electrolytes, dye-sensitized oxide semiconductors provide a visible light-absorbing photoanode that can be coupled to various cathodes for solar fuel production. Understanding the kinetics of electron transfer processes in these photoanodes is important for improving the system efficiency. Array electrodes consisting of vertically aligned, crystalline TiO<sub>2</sub> nanowires have been developed for conventional, nonaqueous dye cells to accelerate electron transport between the electrode/electrolyte interface, where charge injection occurs, and the transparent conductor back electrode contact. Here, we report a kinetic study of electron transport and recombination in dye-sensitized TiO<sub>2</sub> nanowire array electrodes in aqueous media and compare them to more typical mesoporous nanoparticle electrodes. Intensity-modulated photocurrent spectroscopy and intensity-modulated photovoltage spectroscopy were used to measure electron diffusion coefficients and recombination lifetimes. At the same light intensity, the electron diffusion coefficient in rutile TiO<sub>2</sub> nanowire array electrodes was 1–2 times faster, and the electron recombination lifetime was one order of magnitude longer than that in nanoparticle-based anatase photoelectrodes. However, the overall photoinjected electron density was lower with the nanowire array electrodes because of their lower surface area and low coverage of dye molecules. These results suggest that higher surface area nanowire array electrodes coupled with strongly absorbing dyes could potentially improve the efficiency of solar fuel systems based on dye-sensitized photoanodes.



## INTRODUCTION

With the growing demand for renewable energy, an important goal is to develop efficient, low-cost systems that can produce fuels directly from sunlight. Dye-sensitized semiconductor photoelectrodes provide a platform for integrating light-absorbing molecules with catalysts for the anodic and cathodic reactions involved in solar fuel production. In water-splitting dye-sensitized photoelectrochemical cells (WS-DSPECs)<sup>1–4</sup> strongly absorbing sensitizers have been coupled to efficient water-splitting catalysts to achieve monochromatic incident photon-to-electron current efficiencies (IPCEs) approaching 25%.<sup>5</sup> Conventionally, mesoporous TiO<sub>2</sub> or core–shell SnO<sub>2</sub>/TiO<sub>2</sub> nanoparticle films have been used as the semiconductor material for photoanodes.<sup>5–9</sup> While the majority of these studies have involved the mesoporous electrode structures originally developed for regenerative dye-sensitized solar cells (DSSCs),<sup>10</sup> TiO<sub>2</sub> nanowire array electrodes have also been studied, both for nonaqueous DSSCs<sup>11–13</sup> and for water-splitting photoanodes in which TiO<sub>2</sub> acts as the light absorber.<sup>14,15</sup> In both cases, experiments have shown that the one-dimensional architecture of the TiO<sub>2</sub> nanowire arrays increases the diffusion coefficient for transport of photo-generated electrons to the transparent conductor back contact of the photoanode.

A previous study by Feng et al.<sup>11</sup> investigated the charge transport properties of rutile TiO<sub>2</sub> nanowire arrays in nonaqueous DSSCs by using intensity-modulated photocurrent spectroscopy (IMPS) and intensity-modulated photo-

voltage spectroscopy (IMVS). Those experiments showed that the nanowire array architecture increased the electron diffusion coefficient but also increased the charge recombination rate at the nanowire–electrolyte interface. In nonaqueous DSSCs, iodide/triiodide anions are used in the electrolyte to shuttle redox equivalents, and the electrolyte permeates the nanowire array. Although photoinjected electrons diffuse rapidly within the nanowires, the increased recombination rate with triiodide results in no significant change in the efficiency of charge collection. In contrast, in the WS-DSPEC, the primary loss mechanism is charge recombination between photoinjected electrons and oxidized dye molecules adsorbed onto the semiconductor surface.<sup>6,16,17</sup> Charge recombination at the semiconductor/electrolyte interface may not be as significant a problem for WS-DSPECs, since the concentration of oxidized species (i.e., molecular oxygen) in the electrolyte is low. This question motivates the current study of electron transfer kinetics in the nanowire array architecture.

Xu et al.<sup>16,18</sup> recently reported a full kinetic model for TiO<sub>2</sub> nanoparticle photoanodes in WS-DSPECs. IMVS and IMPS

Received: July 31, 2020

Revised: September 12, 2020

Published: September 15, 2020



data were used to measure the rates of electron transport, charge recombination, and dye regeneration by a hydroquinone reductant in the aqueous electrolyte. The hydroquinone was used at low concentration to mimic the slow kinetics of the catalytic water oxidation reaction. Using this model, the performance of the WS-DSPEC was then simulated using a range of rates for charge recombination, electron diffusion, and catalyst turnover. The results showed that the IPCE of WS-DSPECs could be improved by accelerating electron diffusion relative to the best reported values for conventional mesoporous electrode architectures.

We report here photoelectrochemical experiments that compare the electron transport properties of conventional anatase TiO<sub>2</sub> nanoparticle electrodes (TiO<sub>2</sub>-NPs) and rutile TiO<sub>2</sub> nanowire array electrodes (TiO<sub>2</sub>-NWs). IMPS and IMVS were used to obtain electron diffusion coefficients and recombination lifetimes, respectively. The results show that the TiO<sub>2</sub> nanowire array architecture facilitates faster electron diffusion and potentially reduce charge recombination on the surface of TiO<sub>2</sub>.

## EXPERIMENTAL SECTION

**Photoanode Preparation.** Bis(2,2'-bipyridine)(4,4'-diphosphonato-2,2'-bipyridine)ruthenium(II) bromide, RuP, was synthesized as previously described and used as the molecular sensitizer.<sup>19,20</sup> Anatase TiO<sub>2</sub>-NPs were prepared by a previously reported procedure.<sup>21</sup> The synthesis of rutile TiO<sub>2</sub>-NW arrays was adapted from the method developed by Liu et al.<sup>12</sup> Deionized water (22.5 mL) was mixed with concentrated hydrochloric acid (36.5–38 wt %, 22.5 mL) and stirred for 5 min. After the addition of titanium butoxide (97%, 0.75 mL), the mixture was stirred for 5 min before loading into a Teflon-lined stainless-steel autoclave, with two pieces of clean fluorine-doped tin oxide (FTO) on glass substrates (TEC-8, Hartford glass company). The substrates were tilted in the autoclave with the FTO-coated side facing downward. The autoclave was heated at 200 °C for 4 h and then cooled to room temperature. The growth solution was replaced with a new mixture, which was made by first mixing deionized water (18.75 mL), saturated aqueous sodium chloride solution (3.75 mL), and concentrated hydrochloric acid (22.5 mL) for 5 min and then adding titanium butoxide (0.75 mL) and stirring for 5 min. The autoclave was then heated at 150 °C for 20 h. After cooling to room temperature, the FTO-coated glass substrates, now covered by the nanowire array, were taken out, thoroughly rinsed with deionized water, allowed to dry in ambient air, and stored in a 70 °C oven for at least 20 min. The electrodes were then sensitized by immersing in 0.1 mM RuP in ethanol solution at room temperature in the dark for 20 h. Following sensitization, the electrodes were thoroughly rinsed with ethanol and dried in ambient air.

**Characterization and Measurements.** Scanning electron microscopy (SEM) images were obtained using a Quanta 600 FEG environmental scanning electron microscope. X-ray diffraction (XRD) patterns of the nanowire arrays were recorded on a Rigaku X-ray powder diffractometer (SmartLab SE). Transmission electron microscopy (TEM) and selected area electron diffraction (SAED) experiments were performed on a JEOL JEM-F200.

All photoelectrochemical measurements were carried out using a Metrohm Autolab potentiostat (PGSTAT128N). The working electrodes were placed in an electrochemical cell, with a Ag/AgCl (3 M NaCl) reference electrode and a Pt wire

counter electrode. The electrochemical cell was illuminated using a 470 nm LED (LDC470, Metrohm). The light intensity was monitored using a silicon photodiode power sensor (Thorlabs, S130C). The electrolyte was 0.1 M acetic acid/sodium acetate (pH 4.8, degassed by purging with argon).

The number density of photoinjected electrons was measured by charge extraction experiments, in 0.1 M acetate buffer with 3 mM hydroquinone. The photocurrent was measured immediately after the light illuminating the electrodes was switched off, at an applied bias of 0.3 V versus Ag/AgCl. The photoinjected electron density was determined by integrating the photocurrent decay over time after subtracting the dark background current and divided by the product of electrode thickness, volume percentage of TiO<sub>2</sub> in the electrode film, and the absolute value of elementary charge.

The LED light source in impedance spectroscopy experiments was driven using an Autolab LED Driver. The amplitude of the sinusoidal perturbation was 10% of the steady-state light intensity. IMPS experiments were conducted in the 0.1 M acetic acid/sodium acetate buffer with 3 mM hydroquinone, at an applied bias of 0.3 V versus Ag/AgCl. The photocurrent response was recorded over the frequency range of 1000 to 1 Hz of the light perturbation. IMVS experiments were conducted in the 0.1 M acetic acid/sodium acetate buffer, under open-circuit conditions, at an applied frequency range from 400 to 1 Hz.

## RESULTS AND DISCUSSION

TiO<sub>2</sub>-NPs were prepared by doctor blading the as-prepared anatase TiO<sub>2</sub> nanoparticle paste onto FTO substrates. SEM images (Figure S1) of the electrode cross section and surface show the mesoporous structure with an average electrode thickness of 2.9 μm. Rutile TiO<sub>2</sub>-NW arrays were synthesized hydrothermally on the FTO-glass electrodes. As shown in the cross-sectional view SEM image of TiO<sub>2</sub>-NWs (Figure 1a), the nanowires are vertically oriented with respect to the FTO substrate. The top view SEM image (Figure 1b) shows that each nanowire with a square-shaped tip is a bundle consisting of even thinner individual nanowires. The average thickness of the nanowire array electrodes was 3.3 μm. XRD patterns (Figure 1c) identified the phase of the nanowires as rutile, with the strongest diffraction from the (101) and (002) reflections.

Figure 2a shows a TEM image of a nanowire and SAED patterns collected along the length of the same nanowire. The sharp spot diffraction patterns indicate that each region sampled is crystalline and that the three regions share a common <101> growth direction. Figure 2b presents one of the SAED patterns, approximately oriented along the 101 zone axis orientation, and with the individual reflections labeled. The (101) lattice spacing was measured to be 0.25 nm (shown in Figure S2), in good agreement with the lattice spacing in rutile TiO<sub>2</sub> (0.248 nm). The presence of strong (101) and (002) reflections in the XRD pattern (Figure 1c) suggests that nanowires grow in both <101> and <001> orientations in the arrays, in contrast to earlier reports<sup>11,12</sup> of predominantly <001> orientation.

The porosity of the electrodes, defined as the ratio of the volume of pores to the geometric volume of the electrode film, was estimated by mass and geometry measurements. The volume of the film, which consists of the volume of pores and the volume of TiO<sub>2</sub>, was determined by measuring the dimensions of the film. The volume of TiO<sub>2</sub> was measured as the ratio of the mass to the density of rutile or anatase TiO<sub>2</sub>.

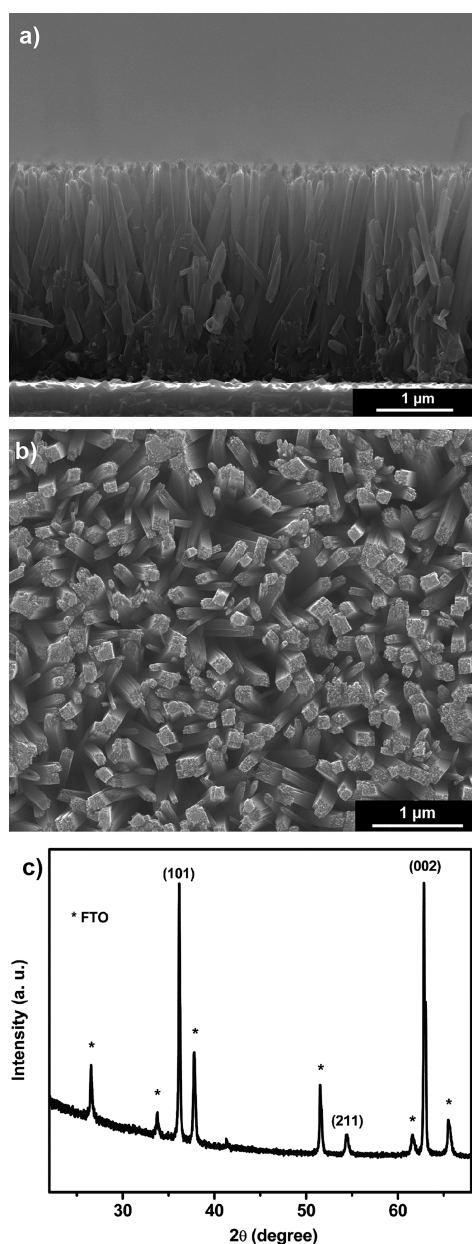


**Figure 1.** (a) Cross-sectional view and (b) top view SEM images of TiO<sub>2</sub>-NWs. (c) XRD pattern of TiO<sub>2</sub>-NWs on the FTO substrate (FTO reflections are labeled by asterisks).

The porosity of the films was thus measured to be  $66 \pm 11\%$  for TiO<sub>2</sub>-NPs and  $58 \pm 17\%$  for TiO<sub>2</sub>-NWs.

**Photoinjected Electron Density.** The short-circuit photoinjected electron density for dye-sensitized TiO<sub>2</sub> in NP and NW electrodes was obtained from charge extraction experiments. Working electrodes were held at 0.3 V (versus Ag/AgCl) under steady-state illumination. This is essentially a short-circuit condition because the current density is not limited by the applied potential (Figure S3). Immediately after the incident light was switched off at  $t = 0$ , the photocurrent decay was measured. Assuming that charge recombination was minimal on the microsecond timescale of charge collection, the photoinjected electron density in the TiO<sub>2</sub> nanostructures could be determined from the expression  $n = J_{SC} \tau / [d(1 - P)q]$ ,<sup>22–24</sup> where  $J_{SC}$  is the photocurrent density at short-circuit,

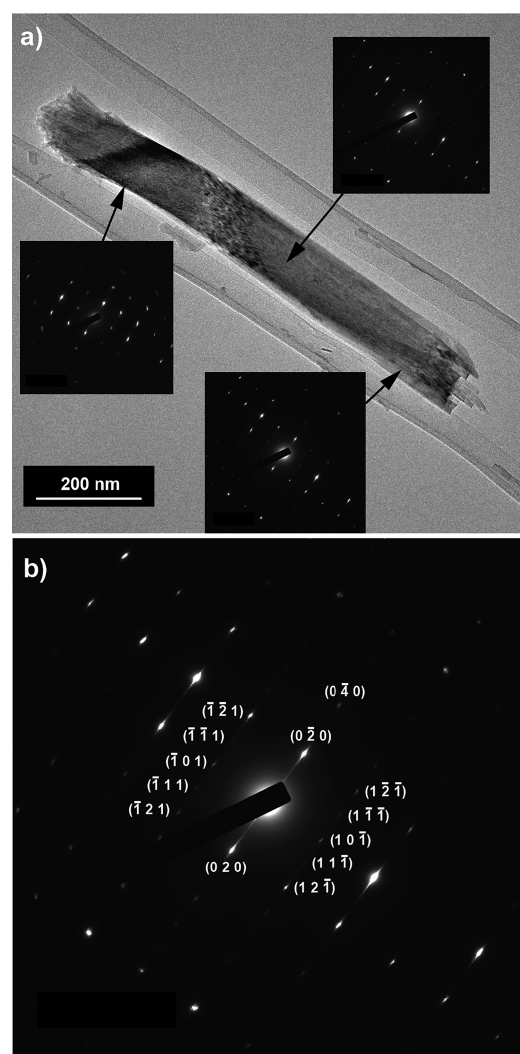


**Figure 2.** (a) TEM image of a TiO<sub>2</sub> nanowire; insets show SAED patterns of different areas on the same nanowire, and (b) enlarged SAED pattern with Miller indices.

$d$  is the thickness of the TiO<sub>2</sub> film,  $P$  is the porosity, and  $q$  is the absolute value of elementary charge.

The photoelectron density in dye-sensitized TiO<sub>2</sub>-NPs and TiO<sub>2</sub>-NWs over a range of incident light intensities is displayed in Figure 3. Within the testing range, the photoinduced

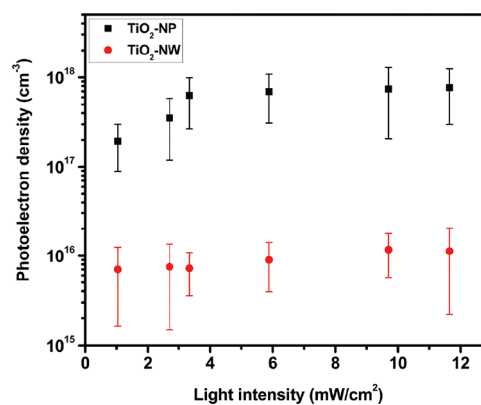


**Figure 3.** Photoelectron density in TiO<sub>2</sub>-NPs (black squares) and in TiO<sub>2</sub>-NWs (red circles) at different incident light intensities.

electron density in TiO<sub>2</sub>-NPs increases with increasing light intensity and tends to saturate at  $7 \times 10^{17} \text{ cm}^{-3}$ , but the electron density of TiO<sub>2</sub>-NWs is roughly constant, with an average value of  $9 \times 10^{15} \text{ cm}^{-3}$ . The electron density generated by steady-state illumination of dye-sensitized TiO<sub>2</sub>-NPs is higher than that in dye-sensitized TiO<sub>2</sub>-NWs by 1–2 orders of magnitude. We attribute this difference to the fact that surface coverage of dye molecules for TiO<sub>2</sub>-NPs is larger than that for TiO<sub>2</sub>-NWs (Figure S4), which stems from the higher porosity and higher surface area of TiO<sub>2</sub>-NPs. The photoelectron density in TiO<sub>2</sub>-NWs does not show a strong dependence of the intensity of incident illumination, possibly because of the fast charge transfer process happening in the nanowire structure. Once injected into the conduction band of the TiO<sub>2</sub> nanowires, electrons diffuse and are collected rapidly at the back contact, and so, their steady-state density remains low.

**IMPS.** Figure 4 shows IMPS Nyquist plots of dye-sensitized TiO<sub>2</sub>-NP and TiO<sub>2</sub>-NW photoelectrodes. The magnitude of

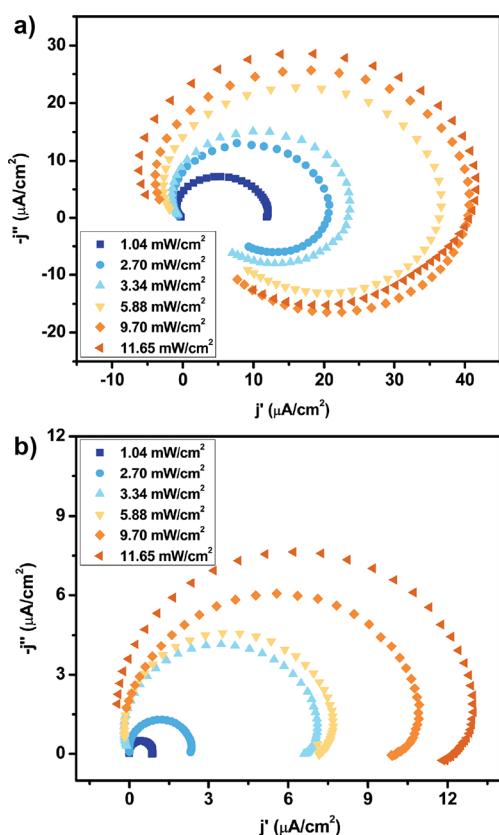


**Figure 4.** IMPS Nyquist plots of dye-sensitized (a) TiO<sub>2</sub>-NP and (b) TiO<sub>2</sub>-NW photoelectrodes.

the IMPS response in both cases scales positively with incident light intensity. In the Nyquist plot of the NP electrode (Figure 4a), we observe that the curves extend into the fourth quadrant. This suggests that there are inductive effects in the mesoporous nanoparticle film, which can arise from loop currents in the interconnected network of nanoparticles.<sup>25</sup> The TiO<sub>2</sub> NW array electrode, on the other hand, does not contain closed loops, and therefore, no inductive effect was observed.

Figure 5 displays Bode plots of dye-sensitized TiO<sub>2</sub>-NP and TiO<sub>2</sub> NW photoelectrodes. In both plots, we observe a peak shift toward high frequency as the intensity of illumination increases. At the peak of each curve in the IMPS Bode plots,

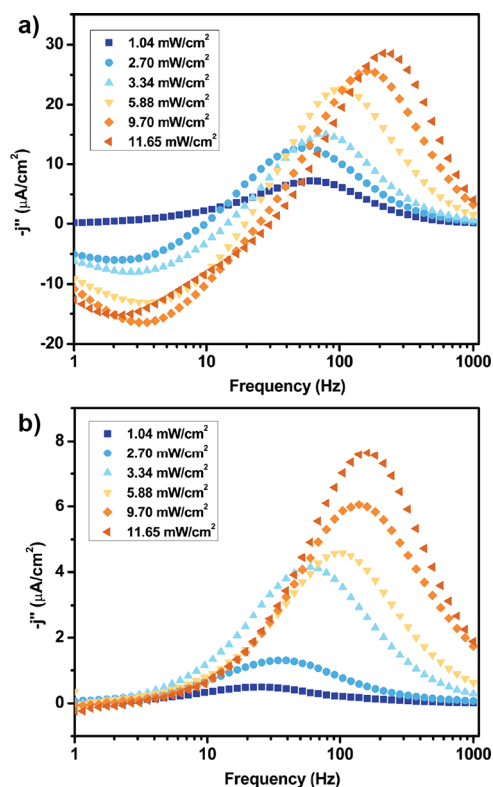


**Figure 5.** IMPS Bode plots of (a) TiO<sub>2</sub>-NPs and (b) TiO<sub>2</sub>-NWs.

the frequency is denoted as  $f_{\text{IMPS}}$ , which is related to the electron transport time constant  $\tau_{\text{tr}} = 1/f_{\text{IMPS}}$ . This time constant can be used to estimate the electron diffusion coefficient by using the relation  $D_n = d^2/(2.35\tau_{\text{tr}})$ ,<sup>26</sup> where  $d$  is the thickness of the TiO<sub>2</sub> electrode film.

Figure 6a shows plots of the calculated electron diffusion coefficients ( $D_n$ ) in each TiO<sub>2</sub> nanostructure as a function of incident light intensity. At low illumination intensities, the diffusion coefficients in TiO<sub>2</sub>-NP are slightly larger than those in TiO<sub>2</sub>-NW films, but the uncertainty in the measurements (especially for the NW films) is large. At higher light intensity, we observe that the diffusion coefficient in TiO<sub>2</sub>-NWs is approximately a factor of two greater than that in the TiO<sub>2</sub>-NP film. The relation between electron diffusion coefficients and photoinjected electron density is shown in Figure 6b. In both TiO<sub>2</sub> nanostructures, diffusion coefficients increase with increasing photoinjected electron density. The result is consistent with previous studies of dye-sensitized porous nanocrystalline TiO<sub>2</sub>.<sup>24,27</sup> Even though the photoelectron density in TiO<sub>2</sub>-NW is more than one order of magnitude lower than that in TiO<sub>2</sub>-NP, the diffusion coefficient in TiO<sub>2</sub>-NW is still higher.

The difference in electron diffusion coefficients in two types of TiO<sub>2</sub> nanostructures indicates that TiO<sub>2</sub>-NWs support faster electron collection at the FTO back contact. This result is consistent with earlier measurements in nonaqueous DSSCs<sup>11</sup> and can be attributed to the crystallinity and the architecture of TiO<sub>2</sub>. The high crystallinity eliminates defects associated with trap states that inhibit effective transport of electrons to the back contact. In addition, the crystalline nanowires provide a direct pathway for electron transport that does not entail a tortuous path through interparticle connections in the mesoporous NP film.

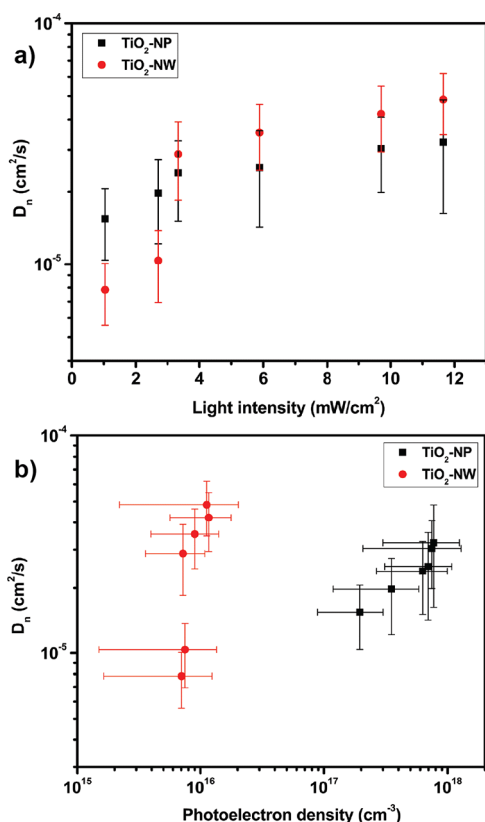


**Figure 6.** Electron diffusion coefficient ( $D_n$ ) in TiO<sub>2</sub>-NPs (black squares) and in TiO<sub>2</sub>-NWs (red circles) as a function of (a) incident light intensity and of (b) photoelectron density.

**IMVS.** In Nyquist plots of IMVS data from dye-sensitized TiO<sub>2</sub>-NP (Figure 7a) and NW (Figure 7b) photoelectrodes, we do not observe a discernible dependency of the IMVS response on the intensity of the incident illumination. The magnitude of the IMVS response is larger with TiO<sub>2</sub>-NP photoelectrodes than that in TiO<sub>2</sub>-NW photoelectrodes. This is consistent with the higher loading of sensitizer molecules in the mesoporous nanoparticle films.

IMVS Bode plots (Figure 8a,b) show the relationship between the imaginary component of the photovoltage response and the frequency. At the peak of each curve, the frequency is denoted as  $f_{\text{IMVS}}$ . We observe that  $f_{\text{IMVS}}$  increases with increasing light intensity, indicating faster charge recombination at higher light intensity. The frequency can be converted to a charge recombination lifetime by the relation  $\tau_{\text{rec}} = 1/f_{\text{IMVS}}$ .<sup>28</sup>

The electron recombination lifetimes ( $\tau_{\text{rec}}$ ) for dye-sensitized TiO<sub>2</sub>-NP and TiO<sub>2</sub>-NW photoelectrodes are plotted against the incident light intensity in Figure 9a. In both cases,  $\tau_{\text{rec}}$  decreases with increasing light intensity. Comparing the electron lifetime at the same light intensity in each morphology of the TiO<sub>2</sub> nanostructure,  $\tau_{\text{rec}}$  in the TiO<sub>2</sub>-NW photoelectrode is about one order of magnitude longer than that in the TiO<sub>2</sub>-NP photoelectrode. In Figure 9b, the electron recombination lifetime is plotted as a function of photoelectron density. As indicated by the decreasing recombination lifetime, the electron recombination rate increases with increasing photoelectron density. The observed longer recombination lifetime in TiO<sub>2</sub>-NW electrodes thus arises in large part from the lower photoelectron density. It is therefore difficult to make a direct comparison between the electron recombination lifetimes in

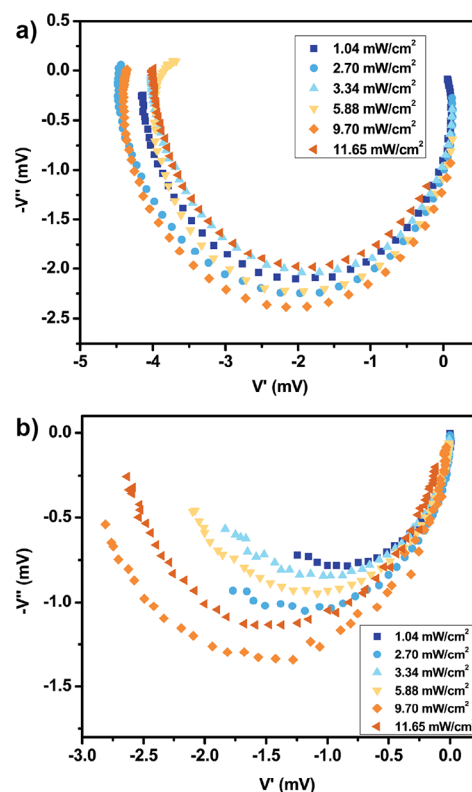


**Figure 7.** IMVS Nyquist plots of dye-sensitized (a) TiO<sub>2</sub>-NP and (b) TiO<sub>2</sub>-NW photoelectrodes.

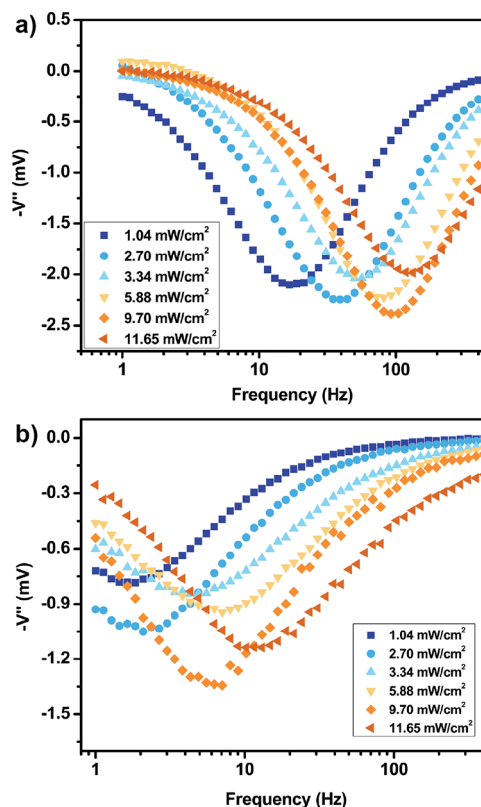


**Figure 8.** IMVS Bode plots of dye-sensitized (a) TiO<sub>2</sub>-NP and (b) TiO<sub>2</sub>-NW photoelectrodes.

each of the TiO<sub>2</sub> nanostructures because of the large difference in the photogenerated electron density. However, based on the

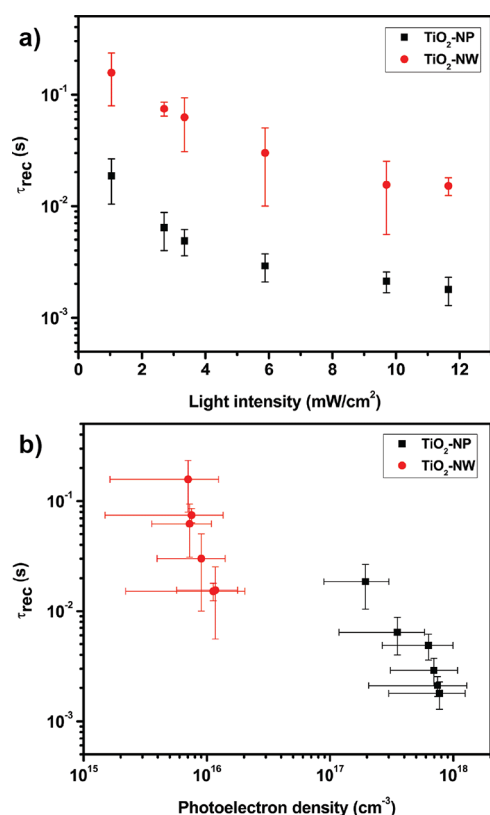


**Figure 9.** Electron recombination lifetime ( $\tau_{\text{rec}}$ ) in dye-sensitized  $\text{TiO}_2\text{-NP}$  (black squares) and  $\text{TiO}_2\text{-NW}$  (red circles) photoelectrodes as a function of (a) incident light intensity and of (b) photoelectron density.

finding that the nanowire structure supports fast electron diffusion, we predict that  $\text{TiO}_2$  nanowire arrays could potentially reduce the electron recombination process in WS-DSPECs. In the nonaqueous DSSCs, charge recombination occurs primarily between photoinjected electrons and triiodide ions in the electrolyte. In the aqueous system, however, charge recombination occurs primarily between trapped electrons and oxidized dye molecules on the  $\text{TiO}_2$  surface. The faster electron transport can increase the charge collection rate at the back contact and thus reduce charge accumulation on the  $\text{TiO}_2$  surface.

## CONCLUSIONS

We have measured electron diffusion coefficients and charge recombination lifetimes of dye-sensitized  $\text{TiO}_2$  nanoparticle and nanowire array electrodes, using IMPS and IMVS, respectively, in aqueous electrolytes. In the IMPS experiments, a small amount of hydroquinone was added in the electrolyte as an electron donor to mimic dye regeneration by an efficient oxygen evolution catalyst in a WS-DSPEC anode. Electron diffusion coefficients obtained from IMPS at the same light intensity showed that electron transport is faster in dye-sensitized nanowire array electrodes even at lower photo-injected electron density. Electron recombination lifetimes at the same light intensity obtained from IMVS indicate that electron recombination is slower in nanowire array electrodes, although the lower photo-injected electron density is clearly an important factor in slow recombination. The crystallinity and vertical alignment of the nanowires facilitates electron transport by eliminating electron trap states and providing a

direct electron transport pathway to the electrode back contact. The fast electron transport property of the nanowire structure could potentially lower the charge recombination rate for photoanodes in the aqueous electrolyte of WS-DSPECs. The results provide experimental evidence of the possibility of increasing the efficiency of WS-DSPECs by changing the architecture of the photoelectrode. While these results are promising, the realization of practical water splitting dye cells by using  $\text{TiO}_2$  nanowire array electrodes will require a technique for growing higher surface area nanowires that can increase the amount of adsorbed sensitizer, as indicated by previous studies,<sup>29–32</sup> to match that of conventional mesoporous  $\text{TiO}_2$  films. Another direction for future success of the  $\text{TiO}_2$  nanowire structure in a water-splitting dye cell is to employ dye molecules that absorb light more strongly and have been shown to increase the efficiency of nonaqueous DSSCs.<sup>33–35</sup>

## ASSOCIATED CONTENT

### Supporting Information

The Supporting Information is available free of charge at <https://pubs.acs.org/doi/10.1021/acs.jpcc.0c07036>.

Electron micrographs of photoelectrode films, high-resolution TEM image of  $\text{TiO}_2$  nanowire, J–V curves of photoelectrodes, and dye surface coverage data (3 pp.) (PDF)

## AUTHOR INFORMATION

### Corresponding Author

**Thomas E. Mallouk** – Department of Chemistry, University of Pennsylvania, Philadelphia, Pennsylvania 19104, United States; [orcid.org/0000-0003-4599-4208](https://orcid.org/0000-0003-4599-4208); Email: [mallouk@sas.upenn.edu](mailto:mallouk@sas.upenn.edu)

### Authors

**Langqiu Xiao** – Department of Chemistry, University of Pennsylvania, Philadelphia, Pennsylvania 19104, United States

**Yanan Yu** – Department of Materials Science and Engineering, University of Pennsylvania, Philadelphia, Pennsylvania 19104, United States; Institute for Sustainability and Energy, Northwestern University, Evanston, Illinois 60208, United States

**Emma L. Schultz** – Department of Chemistry, University of Pennsylvania, Philadelphia, Pennsylvania 19104, United States

**Eric A. Stach** – Department of Materials Science and Engineering, University of Pennsylvania, Philadelphia, Pennsylvania 19104, United States; [orcid.org/0000-0002-3366-2153](https://orcid.org/0000-0002-3366-2153)

Complete contact information is available at: <https://pubs.acs.org/10.1021/acs.jpcc.0c07036>

### Notes

The authors declare no competing financial interest.

## ACKNOWLEDGMENTS

We thank Jarrett D. Dillenburger for the help with XRD experiments. This work was supported by the Office of Basic Energy Sciences, Division of Chemical Sciences, Geosciences, and Energy Biosciences, Department of Energy, under contract SC-0019781, and by the Vagelos Institute for Energy Science and Technology at the University of Pennsylvania. This work was performed in part at the Singh Center for Nanotechnology

at the University of Pennsylvania, a member of the National Nanotechnology Coordinated Infrastructure (NNCI) network, which is supported by the National Science Foundation (Grant NNCI-1542153). The authors gratefully acknowledge use of facilities and instrumentation supported by NSF through the University of Pennsylvania Materials Research Science and Engineering Center (MRSEC) (DMR-1720530).

## REFERENCES

- (1) Yun, S.; Vlachopoulos, N.; Qurashi, A.; Ahmad, S.; Hagfeldt, A. Dye Sensitized Photoelectrolysis Cells. *Chem. Soc. Rev.* **2019**, *48*, 3705–3722.
- (2) Xu, P.; McCool, N. S.; Mallouk, T. E. Water Splitting Dye-Sensitized Solar Cells. *Nano Today* **2017**, *14*, 42–58.
- (3) Brennaman, M. K.; Dillon, R. J.; Alibabaei, L.; Gish, M. K.; Dares, C. J.; Ashford, D. L.; House, R. L.; Meyer, G. J.; Papanikolas, J. M.; Meyer, T. J. Finding the Way to Solar Fuels with Dye-Sensitized Photoelectrosynthesis Cells. *J. Am. Chem. Soc.* **2016**, *138*, 13085–13102.
- (4) Yu, Z.; Li, F.; Sun, L. Recent Advances in Dye-Sensitized Photoelectrochemical Cells for Solar Hydrogen Production Based on Molecular Components. *Energy Environ. Sci.* **2015**, *8*, 760–775.
- (5) Wang, D.; Marquard, S. L.; Troian-Gautier, L.; Sheridan, M. V.; Sherman, B. D.; Wang, Y.; Eberhart, M. S.; Farnum, B. H.; Dares, C. J.; Meyer, T. J. Interfacial Deposition of Ru(II) Bipyridine-Dicarboxylate Complexes by Ligand Substitution for Applications in Water Oxidation Catalysis. *J. Am. Chem. Soc.* **2018**, *140*, 719–726.
- (6) Youngblood, W. J.; Lee, S.-H. A.; Kobayashi, Y.; Hernandez-Pagan, E. A.; Hoertz, P. G.; Moore, T. A.; Moore, A. L.; Gust, D.; Mallouk, T. E. Photoassisted Overall Water Splitting in a Visible Light-Absorbing Dye-Sensitized Photoelectrochemical Cell. *J. Am. Chem. Soc.* **2009**, *131*, 926–927.
- (7) Zhao, Y.; Swierk, J. R.; Megiatto, J. D.; Sherman, B.; Youngblood, W. J.; Qin, D.; Lentz, D. M.; Moore, A. L.; Moore, T. A.; Gust, D.; Mallouk, T. E. Improving the Efficiency of Water Splitting in Dye-Sensitized Solar Cells by Using a Biomimetic Electron Transfer Mediator. *Proc. Natl. Acad. Sci. U. S. A.* **2012**, *109*, 15612–15616.
- (8) Gao, Y.; Ding, X.; Liu, J.; Wang, L.; Lu, Z.; Li, L.; Sun, L. Visible Light Driven Water Splitting in a Molecular Device with Unprecedentedly High Photocurrent Density. *J. Am. Chem. Soc.* **2013**, *135*, 4219–4222.
- (9) Alibabaei, L.; Sherman, B. D.; Norris, M. R.; Brennaman, M. K.; Meyer, T. J. Visible Photoelectrochemical Water Splitting into H<sub>2</sub> and O<sub>2</sub> in a Dye-Sensitized Photoelectrosynthesis Cell. *Proc. Natl. Acad. Sci. U. S. A.* **2015**, *112*, 5899–5902.
- (10) O'Regan, B.; Grätzel, M. A Low-Cost, High-Efficiency Solar Cell Based on Dye-Sensitized Colloidal TiO<sub>2</sub> Films. *Nature* **1991**, *353*, 737–740.
- (11) Feng, X.; Zhu, K.; Frank, A. J.; Grimes, C. A.; Mallouk, T. E. Rapid Charge Transport in Dye-Sensitized Solar Cells Made from Vertically Aligned Single-Crystal Rutile TiO<sub>2</sub> nanowires. *Angew. Chem., Int. Ed.* **2012**, *51*, 2727–2730.
- (12) Liu, B.; Aydil, E. S. Growth of Oriented Single-Crystalline Rutile TiO<sub>2</sub> Nanorods on Transparent Conducting Substrates for Dye-Sensitized Solar Cells. *J. Am. Chem. Soc.* **2009**, *131*, 3985–3990.
- (13) Feng, X.; Shankar, K.; Varghese, O. K.; Paulose, M.; Latempa, T. J.; Grimes, C. A. Vertically Aligned Single Crystal TiO<sub>2</sub> Nanowire Arrays Grown Directly on Transparent Conducting Oxide Coated Glass: Synthesis Details and Applications. *Nano Lett.* **2008**, *8*, 3781–3786.
- (14) Su, J.; Guo, L. High Aspect Ratio TiO<sub>2</sub> Nanowires Tailored in Concentrated HCl Hydrothermal Condition for Photoelectrochemical Water Splitting. *RSC Adv.* **2015**, *5*, 53012–53018.
- (15) Wang, G.; Wang, H.; Ling, Y.; Tang, Y.; Yang, X.; Fitzmorris, R. C.; Wang, C.; Zhang, J. Z.; Li, Y. Hydrogen-Treated TiO<sub>2</sub> Nanowire Arrays for Photoelectrochemical Water Splitting. *Nano Lett.* **2011**, *11*, 3026–3033.
- (16) Xu, P.; Gray, C. L.; Xiao, L.; Mallouk, T. E. Charge Recombination with Fractional Reaction Orders in Water-Splitting Dye-Sensitized Photoelectrochemical Cells. *J. Am. Chem. Soc.* **2018**, *140*, 11647–11654.
- (17) Swierk, J. R.; McCool, N. S.; Mallouk, T. E. Dynamics of Electron Recombination and Transport in Water-Splitting Dye-Sensitized Photoanodes. *J. Phys. Chem. C* **2015**, *119*, 13858–13867.
- (18) Xu, P.; Mallouk, T. E. Charge Transfer Dynamics in Aqueous Dye-Sensitized Photoelectrochemical Cells: Implications for Water Splitting Efficiency. *J. Phys. Chem. C* **2019**, *123*, 299–305.
- (19) Montalti, M.; Wadhwa, S.; Kim, W. Y.; Kipp, R. A.; Schmehl, R. H. Luminescent Ruthenium(II) Bipyridyl-Phosphonic Acid Complexes: pH Dependent Photophysical Behavior and Quenching with Divalent Metal Ions. *Inorg. Chem.* **2000**, *39*, 76–84.
- (20) Trammell, S. A.; Moss, J. A.; Yang, J. C.; Nakhle, B. M.; Slate, C. A.; Odobel, F.; Sykora, M.; Erickson, B. W.; Meyer, T. J. Sensitization of TiO<sub>2</sub> by Phosphonate-Derivatized Proline Assemblies. *Inorg. Chem.* **1999**, *38*, 3665–3669.
- (21) McCool, N. S.; Swierk, J. R.; Nemes, C. T.; Saunders, T. P.; Schmuttenmaer, C. A.; Mallouk, T. E. Proton-Induced Trap States, Injection and Recombination Dynamics in Water-Splitting Dye-Sensitized Photoelectrochemical Cells. *ACS Appl. Mater. Interfaces* **2016**, *8*, 16727–16735.
- (22) Van De Lagemaat, J.; Kopidakis, N.; Neale, N. R.; Frank, A. J. Effect of Nonideal Statistics on Electron Diffusion in Sensitized Nanocrystalline TiO<sub>2</sub>. *Phys. Rev. B Condens. Matter Mater. Phys.* **2005**, *71*, No. 035304.
- (23) Kopidakis, N.; Benkstein, K. D.; Van De Lagemaat, J.; Frank, A. J. Transport-Limited Recombination of Photocarriers in Dye-Sensitized Nanocrystalline TiO<sub>2</sub> Solar Cells. *J. Phys. Chem. B* **2003**, *107*, 11307–11315.
- (24) Kopidakis, N.; Schiff, E. A.; Park, N. G.; Van De Lagemaat, J.; Frank, A. J. Ambipolar Diffusion of Photocarriers in Electrolyte-Filled, Nanoporous TiO<sub>2</sub>. *J. Phys. Chem. B* **2000**, *104*, 3930–3936.
- (25) Von Hauff, E. Impedance Spectroscopy for Emerging Photovoltaics. *J. Phys. Chem. C* **2019**, *123*, 11329–11346.
- (26) Van de Lagemaat, J.; Frank, A. J. Nonthermalized Electron Transport in Dye-Sensitized Nanocrystalline TiO<sub>2</sub> Films: Transient Photocurrent and Random-Walk Modeling Studies. *J. Phys. Chem. B* **2001**, *105*, 11194–11205.
- (27) Schlichthörl, G.; Park, N. G.; Frank, A. J. Evaluation of the Charge-Collection Efficiency of Dye-Sensitized Nanocrystalline TiO<sub>2</sub> Solar Cells. *J. Phys. Chem. B* **1999**, *103*, 782–791.
- (28) Schlichthörl, G.; Huang, S. Y.; Sprague, J.; Frank, A. J. Band Edge Movement and Recombination Kinetics in Dye-Sensitized Nanocrystalline TiO<sub>2</sub> Solar Cells: A Study by Intensity Modulated Photovoltage Spectroscopy. *J. Phys. Chem. B* **1997**, *101*, 8141–8155.
- (29) Law, M.; Greene, L. E.; Johnson, J. C.; Saykally, R.; Yang, P. Nanowire Dye-Sensitized Solar Cells. *Nat. Mater.* **2005**, *4*, 455–459.
- (30) Wu, W. Q.; Xu, Y. F.; Su, C. Y.; Kuang, D. B. Ultra-Long Anatase TiO<sub>2</sub> Nanowire Arrays with Multi-Layered Configuration on FTO Glass for High-Efficiency Dye-Sensitized Solar Cells. *Energy Environ. Sci.* **2014**, *7*, 644–649.
- (31) Hoang, S.; Gao, P. X. Nanowire Array Structures for Photocatalytic Energy Conversion and Utilization: A Review of Design Concepts, Assembly and Integration, and Function Enabling. *Adv. Energy Mater.* **2016**, *6*, 1600683.
- (32) Ni, S.; Wang, D.; Guo, F.; Jiao, S.; Zhang, Y.; Wang, J.; Wang, B.; Yuan, L.; Zhang, L.; Zhao, L. Efficiency Improvement of TiO<sub>2</sub> Nanowire Arrays Based Dye-Sensitized Solar Cells through Further Enhancing the Specific Surface Area. *J. Cryst. Growth* **2019**, *505*, 62–68.
- (33) Zhang, X.; Xu, Y.; Giordano, F.; Schreier, M.; Pellet, N.; Hu, Y.; Yi, C.; Robertson, N.; Hua, J.; Zakeeruddin, S. M.; Tian, H.; Grätzel, M. Molecular Engineering of Potent Sensitizers for Very Efficient Light Harvesting in Thin-Film Solid-State Dye-Sensitized Solar Cells. *J. Am. Chem. Soc.* **2016**, *138*, 10742–10745.

(34) Higashino, T.; Imahori, H. Porphyrins as Excellent Dyes for Dye-Sensitized Solar Cells: Recent Developments and Insights. *Dalton Trans.* **2015**, *44*, 448–463.

(35) Alexy, E. J.; Yuen, J. M.; Chandrasher, V.; Diers, J. R.; Kirmaier, C.; Bocian, D. F.; Holten, D.; Lindsey, J. S. Panchromatic Absorbers for Solar Light-Harvesting. *Chem. Commun.* **2014**, *50*, 14512–14515.